

Macroscopic production of highly nuclear-spin-polarized molecules from IR-excitation and photodissociation of molecular beams

C. S. Kannis^{a,b}, T. P. Rakitzis^{b,c,*}

^a*Institute for Nuclear Physics, Forschungszentrum Jülich, 52425 Jülich, Germany*

^b*University of Crete, Department of Physics, Herakleio, Greece*

^c*Foundation for Research and Technology Hellas, Institute of Electronic Structure and Laser, N. Plastira 100, Heraklion, Crete, Greece, GR-71110*

Abstract

Pure, highly nuclear-spin-polarized molecules have only been produced with molecular beam-separation methods, with production rates up to $\sim 3 \times 10^{12} \text{ s}^{-1}$. Here, we propose the production of spin-polarized molecular photofragments from the IR-excitation and photodissociation of molecular beams, with production rates approaching the tabletop-IR-laser photon fluxes of 10^{21} s^{-1} . We give details on the production of spin-polarized molecular hydrogen and water isotopes, from formaldehyde and formic acid beams, respectively. Macroscopic quantities of these molecules are important for NMR signal enhancement, and for the needs of a nuclear fusion reactor, to increase the D-T or D-³He unpolarized nuclear fusion cross section by $\sim 50\%$.

Keywords: nuclear-spin-polarized molecules, molecular beams, IR excitation, photodissociation, molecular hyperpolarization

2010 MSC: 00-01, 99-00

1. Introduction

The production of nuclear spin polarization is important in several fields, including the study of spin-dependent effects in particle and nuclear

*Corresponding author

URL: ptr@iesl.forth.gr (T. P. Rakitzis)

physics [1], and in applications of solid-state hyperpolarized nuclear magnetic resonance (NMR) [2, 3, 4]. However, current methods for producing highly spin-polarized molecules, such as molecular-beam separation techniques, polarization through “brute force” cryogenic cooling, dynamic nuclear polarization (DNP), and pulsed-laser excitation of molecular beams, have significant production and polarization limitations for many applications.

“Brute force” cryogenic cooling of solid D_2 to 35 mK in a 14.5 T field, produces a polarization of only about 13% [5]. For 100% polarized nuclei, The D-T and D- ^3He nuclear-fusion reaction cross sections are enhanced by 50% [6], and may increase the reactor efficiency by $\sim 75\%$ [7]. A GW nuclear fusion reactor will need $\sim 10^{21} \text{ s}^{-1}$ of 100% polarized D to benefit fully from this effect [8, 9, 10]. Therefore, the “brute force” method cannot produce sufficiently polarized D for this application.

In DNP, the unpaired electrons in free radicals are highly polarized at low temperature in a magnetic field, and this polarization is transferred to the nuclei of the target sample [11]. This works successfully for a wide range of molecules, however the removal of the radicals, necessary for *in vivo* NMR applications, is difficult and can significantly lower the sample polarization [12].

Molecular-beam separation techniques, using electric or magnetic field gradients, is the only method that can produce pure, $\sim 100\%$ nuclear-spin-polarized molecules, however only microscopic production rates have been demonstrated of $\sim 3 \times 10^{12}$ for ortho- H_2 and $\sim 5 \times 10^{11} \text{ s}^{-1}$ for ortho- D_2 [13], and below $\sim 10^{11}$ for ortho- H_2O [14, 15], many orders of magnitude lower than required for many applications; for example, NMR applications and tests of polarized fusion require production rates of at least 10^{17} s^{-1} .

The single-photon rovibrational excitation of molecular beams with an IR laser pulse [16, 17], followed by transfer of the rotational polarization to the nuclear spin via the hyperfine interaction, has been shown to polarize highly the nuclear spins of isolated molecules. This method of hyperpolarization has been demonstrated for Cl nuclei in HCl molecules [18, 19]. However, a path for high production rates for important nuclei, such as H/D/T, was not shown; also, high polarization was not demonstrated for H isotopes via IR excitation, as the rotational polarization preferentially polarizes the more strongly coupled Cl nucleus first. The biggest problem is that only isolated spin-polarized atoms have been produced with this method, and that the production of spin-polarized molecules (such as H_2 isotopes) have only been

performed by recombining the polarized atoms at a surface [20]; this is a very complicated extra step, which has not been demonstrated at high production rates.

Here, we propose improvements to the rovibrational excitation method that will allow macroscopic production rates of pure, highly-polarized molecules ($\sim 100\%$), at rates that can approach the photon fluxes of the IR excitation step. The improvements are motivated by the recent availability of tabletop tunable, narrow-bandwidth, high-power IR lasers, producing $\sim 10^{21}$ photons s^{-1} [21], and are: (i) optical excitation steps that allow *only* molecules with 100% nuclear polarization to be photodissociated, providing a pure polarization spin filter, and (ii) excitation and polarization of larger molecules which can be photodissociated to yield exclusively polarized molecular photofragments, without needing to recombine polarized atoms; this is particularly important for molecules that are not IR active (such as H_2 isotopes), and cannot be excited directly. Specifically, we propose the IR-excitation of the special cases of formaldehyde (CH_2O) or formic acid (CH_2O_2), which can be photodissociated to yield exclusively the $\text{H}_2 + \text{CO}$ [22] or $\text{H}_2\text{O} + \text{CO}$ [23] channels, respectively. The target molecules (here H_2 or H_2O isotopes) can then be selectively trapped at a surface. Thus, we propose the production of macroscopic quantities of $\sim 100\%$ nuclear-spin-polarized isotopes of hydrogen molecules (H_2 , HD, DT) and water molecules (H_2O , D_2O), which are important for the applications of polarized nuclear fusion and NMR signal enhancement. This production method will surpass conventional beam separation methods by several orders of magnitude, and may approach the photon flux of the IR excitation lasers (details given below).

Below, and in Figs. 1 and 2, we give details on the production of $\sim 100\%$ nuclear-spin-polarized molecules from IR-excitation and photodissociation of CH_2O and CH_2O_2 . The steps are described generally, but specific numbers are given for the case of CH_2O (for production rates of up to 10^{20} s^{-1} spin-polarized H_2):

1. *Slit nozzle supersonic expansion.* Produces a $10\text{ cm} \times 1\text{ cm}$ jet at the laser interaction region (Fig. 1 and [24]), with CH_2O density of $\sim 2 \times 10^{15}$ cm^{-3} (seeded in He) with beam velocity of $\sim 2 \times 10^5$ cm s^{-1} , translational temperature of ~ 1 K and rotational temperature of ~ 3 K, thus cooling about half of the ortho- CH_2O to the ground $J = 0$ state.

2. *IR excitation (step 1).* Transition from the ground state $|\nu = 0, J = 0, m_J = 0\rangle$ to $|\nu', J, m_J = +J\rangle$ with σ_+ light, and $J = 1$ or 2 (Fig. 2). $J = 1$

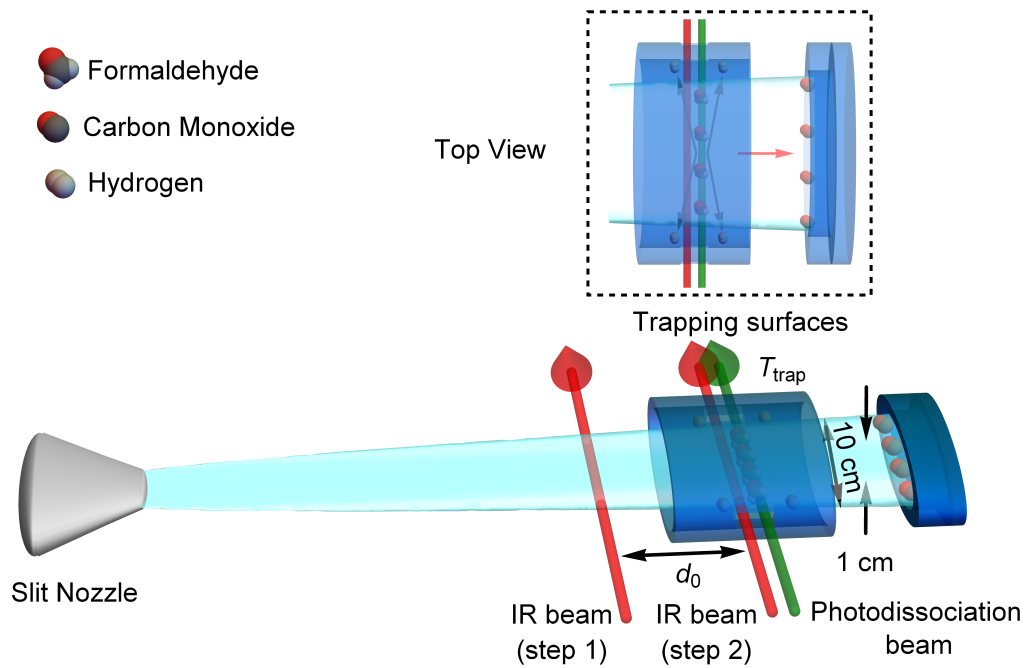


Figure 1: Experimental setup: supersonic expansion of CH_2O or CH_2O_2 gas, followed by IR excitation (step 1), time evolution for time $t_{\text{max}} = d_0/v$, then photodissociation, and trapping of polarized hydrogen or water photofragments at the cold surface.

is used for photoproducts with total nuclear spin $I = 1$ (such as ortho H_2 or H_2O), and $J = 2$ for nuclei with total nuclear spin $I = 3/2$ (such as HD or DT) or 2 (such as ortho D_2 or D_2O), via successive two-photon absorption using STIRAP [25, 26, 27], for which population-transfer efficiency is typically $> 90\%$. The absorption cross sections are $\sim 10^{-16} \text{ cm}^2$ (for $\nu' = \nu_2\nu_5$ at 4581.69 cm^{-1}) and the column density of the ground state is $3 \times 10^{16} \text{ cm}^{-2}$ so that greater than 99% of the 10^{21} s^{-1} IR photons are absorbed (as the 1 MHz laser linewidth is much narrower than the transition linewidth); for lower absorption cross sections, buildup cavities can be used to maximize IR absorption.

3. *Hyperfine polarization beating.* Subsequently, we leave the system to evolve freely, transferring rotational polarization to nuclear polarization, until the population of $|\nu', J, m_J = -J\rangle$ (for $I = 1$ or 2) or $|\nu', J, m_J = -J + 1\rangle$ (for $I = 3/2$) is maximized ($t = t_{max}$). This state is 100% nuclear-spin polarized, due to the conservation of the total angular momentum projection along the quantization axis (hyperfine beatings under similar conditions have been demonstrated for HCl, HD, D_2 [18, 28, 29]). For CH_2O , 16% of the population is 100% nuclear-spin-polarized and is transferred to the $m_J = -1$ state (see Section 2). The total rotational energy transfer and depolarization cross section for the $|J = 1, K = 0, M = 1\rangle$ state in CH_2O is $\sim 3 \times 10^{-15} \text{ cm}^2$ [30] (assuming a collision-energy-independent cross section). For collisional speeds of $\sim 3 \times 10^3 \text{ cm s}^{-1}$, the de-excitation rate is $\sim 10^{-11} \text{ cm}^3 \text{ s}^{-1}$, which, for 10^{15} cm^3 densities, gives a de-excitation time of $\sim 100 \mu\text{s}$; therefore, t_{max} should be significantly less than $100 \mu\text{s}$. In addition, the velocity spread in the supersonic expansion is much less than 10% [31], so that the blurring in the peak of a half an oscillation is less than 1%.

4. *Hyperfine beating stopped.* At $t = t_{max}$, the beam enters a magnetic field of $\sim 1 \text{ mT}$, which stops the hyperfine beating. A sharp magnetic field gradient is necessary to decouple nuclear spin and rotation and minimize the polarization losses. This has been shown in [32] for the case of H_2 molecules; a similar calculation for CH_2O is expected to show similar behavior, and can be performed in future work.

5. *IR excitation (step 2) and photodissociation.* The transition $|\nu', J, m_J = -J\rangle \rightarrow |\nu'', J = 0, m_J = 0\rangle$ (for $I = 1$ or 2) or the $|\nu', J, m_J = -1\rangle \rightarrow |\nu'', J = 1, m_J = +1\rangle$ (for $I = 3/2$), with σ_+ light, so that only the 100% nuclear-spin-polarized state is excited to the highest level. This fully-polarized state is then exclusively photodissociated by the photolysis laser (the lower states not having enough energy to photodissociate). For

CH₂O column density of 3×10^{16} cm⁻² and a photodissociation cross section of 2.5×10^{16} cm² (Fig. 4), more than 99% of the molecules are photodissociated, for laser fluxes of 2×10^{20} photons cm⁻² s⁻¹. The photodissociation cross section for higher vibrational states is shifted to the green from the UV, due to the IR absorption energy of ~ 1 eV. The photodissociation cross section of formic acid at 248 nm, for the CO + H₂O channel, is about 1000 times smaller [33, 34], therefore a buildup cavity will be needed for the photodissociation laser, at 355 nm (for 2 IR photons) or 450 nm (for 4 IR photons), to absorb a large percentage of the photolysis light. The produced H₂ molecules are in J states peaking at ~ 3 [35], and hence a static magnetic field of ~ 1 T is applied in the photodissociation region to prevent significant polarization exchange with J [36]. Notice that the H₂ photodissociation recoil speed is much faster than the beam speed, and therefore the H₂ recoils radially from the photodissociation region and is trapped at the first trapping surface (see Fig. 1); in the contrast, the heavier CO molecules recoil slower than the beam speed, and therefore the CO follows the molecular beam and is trapped with the rest of the unphotodissociated molecules (Fig. 1). In addition, the spatial anisotropy of the CH₂O recoil can be used to direct the H₂ photofragments preferentially towards the trapping surfaces (and less towards the molecules beam direction) [37]. For CH₂O₂ photodissociation, H₂O and CO can be differentially trapped by the trapping surface temperature (as CO melts at 68 K, compared to 273 K for H₂O).

6. *Cold trapping.* More than 90% of the hydrogen or water isotopes reach trapping surfaces (that cover more than 90% of 4π steradians), and are selectively trapped at these cold trapping surfaces with unity sticking probability [38] (the CO mainly follows the beam direction and is trapped elsewhere, with the unphotodissociated molecules (Fig. 1)). The molecules will be trapped as a solid. Spin-polarized HD has been trapped at 4 K for many days [39], whereas spin-polarized H₂O, produced via DNP, was shown to have lifetimes of 10 s of seconds [4] (but pure spin-polarized H₂O should have a longer lifetime).

The product of the efficiencies of the above steps 1-6 is $\sim 10\%$. Therefore, 10^{21} IR photons s⁻¹ will produce and trap an upper limit of 10^{20} s⁻¹ spin-polarized molecules (this can be scaled up with larger laser powers and slit lengths). Future experiments will determine to what extent such production rates can be approached (e.g. the depolarization rates may be higher than assumed here, which will lower the production rate).

We describe in more detail why this method should surpass conventional

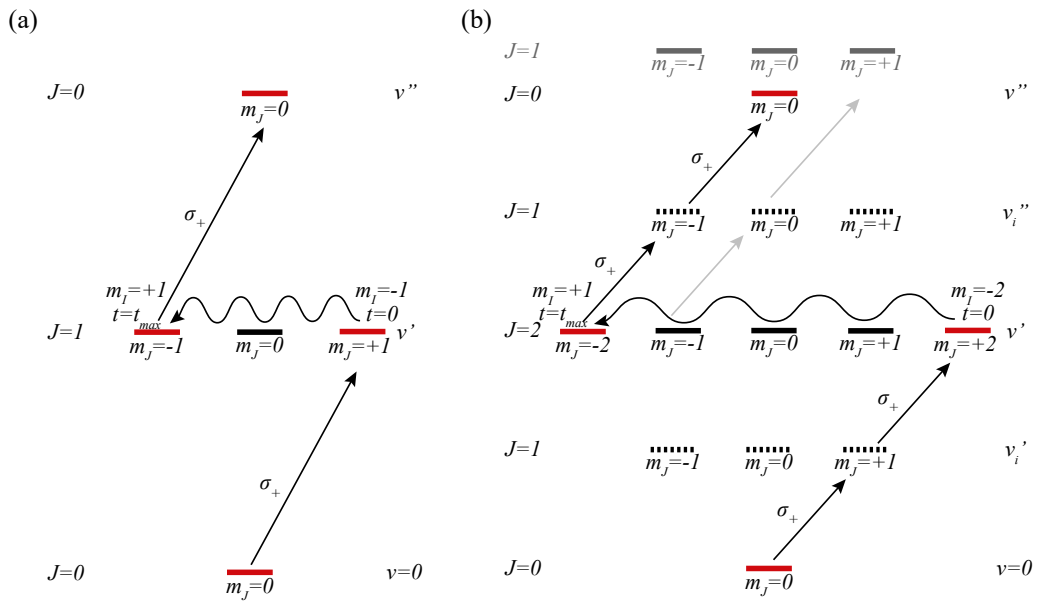


Figure 2: Excitation schemes for production of nuclear spin-polarized molecules with (a) $I = 1$ (e.g. with constituent atoms of D or H_2), and (b) $I = 3/2$ or 2 (e.g. for HD, DT or D_2). The squiggly arrows show rotational polarization reduction $\Delta m_J = -2$ or -4 , associated with nuclear spin increase $\Delta m_I = +2$ or $+4$ (for Figs. 2(a) or 2(b), respectively). Only 100% nuclear-spin-polarized molecules reach the upper state.

methods by several orders of magnitude. Conventional molecular-beam separation methods are based on the differential deflection of the spin-projection states, from a beam with a cross sectional area A , velocity v , and density ρ , with large, localized B-field or E-field gradients, which limit $A \sim 1 \text{ cm}^2$ to be small and localized. However, the beam density must be low enough so that the beam divergence, from collisions, is less than the differential deflections of the target spin-projection states. This constraint limits the beam density to $\rho \sim 10^{11} \text{ cm}^{-3}$ for open-shell atoms [40]. The beam separation occurs over a distance of $\sim 1 \text{ m}$ and on the ms timescale, with a beam velocity v typically in the range $0.2\text{--}2.5 \times 10^5 \text{ cm/s}$. The largest production rate (given by $Av\rho$) for spin-polarized H atoms, which is the most favorable case, has been $\sim 5 \times 10^{16} \text{ H/s}$ [40]. For closed-shell molecules, the production rates are several orders of magnitude lower (as nuclear magnetic moments are $\sim 10^3$ times smaller than electronic ones, due to the $\sim 10^3$ larger mass).

In contrast, the polarization of nuclear spins in a molecular beam, via the IR-excitation method, occurs by the intramolecular transfer of rotational to nuclear polarization, via the hyperfine interaction on the μs timescale, and thus does not require any type of beam separation or external inhomogeneous static fields. The lack of need to spatially separate the spin-states in the molecular beam, the shorter polarization time, and the ability to use a long slit expansion (not possible for conventional beam-separation methods due to the inhomogeneous fields), allow the beam area A and density ρ to be much higher than for beam-separation methods, e.g. $A \sim 10\text{--}100 \text{ cm}^2$, and $\rho \sim 10^{15} \text{ cm}^{-3}$, which are 1-2 and 4 orders of magnitude higher, respectively. This increase in A and ρ potentially allows a total production rate $Av\rho$ of up to $\sim 10^{22} \text{ s}^{-1}$. The production rate is limited by the absorbed photons for the IR-excitation and photodissociation steps: tabletop IR-excitation and photodissociation lasers producing $\sim 10^{21}$ photons s^{-1} are available commercially; industrial-scale lasers can likely reach higher. We note that related arguments were used to predict the production of ultrahigh densities of spin-polarized hydrogen (SPH) atoms from hydrogen halide photodissociation [41], and indeed $10^{19}\text{--}10^{20}$ SPH were observed [42, 43, 44], 8-9 orders higher than those from beam-separation methods; therefore surpassing conventional beam-separation methods by many orders of magnitude is not unprecedented.

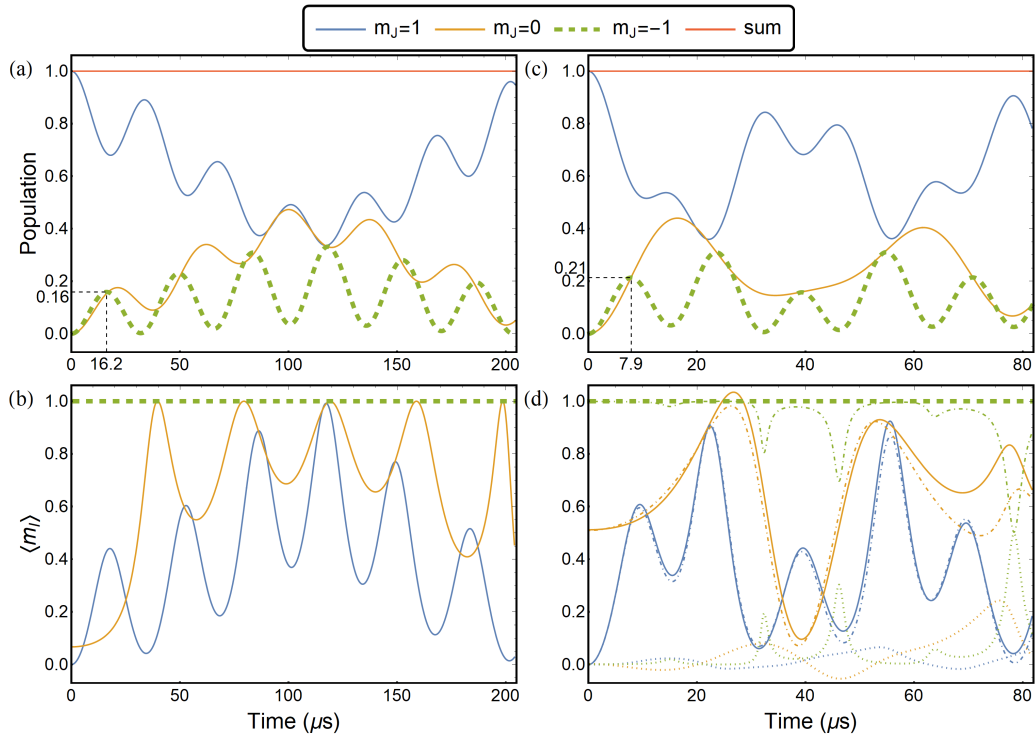


Figure 3: CH₂O (a,b): Population and $\langle m_I \rangle$ of m_J states as function of time. The $m_J = -1$ state reaches 15.9% of the total population at $\sim 16.2 \mu$ s. CHDO (c,d): Population and $\langle m_I \rangle$ of m_J states as function of time. The solid lines (and the dashed thick line) correspond to the total nuclear spin projection, whereas the dash-dotted and dotted lines correspond to $\langle m_{I_D} \rangle$, and $\langle m_{I_H} \rangle$ respectively. The $m_J = -1$ state reaches 21.4% of the total population at 7.9 μ s. By that time, mainly the deuteron is polarized.

2. Production of spin-polarized H₂ (isotopes) from formaldehyde IR excitation and photodissociation

The IR-excitation method depends crucially on transferring a large fraction of the population to the 100% nuclear-spin-polarized state, and in short enough time ($t_{max} \lesssim 30 \mu\text{s}$) to avoid significant depolarization under these conditions. Below, we give a description of the calculation of the polarization transfer and t_{max} for CH₂O and CH₂O₂ isotopes.

The CH₂O ortho states ($I = 1$) are described by $K_{-1} = 1, 3, 5, \dots$ and the para states by $K_{-1} = 0, 2, 4, \dots$ in the notation $J_{K_{-1}K_1}$ [45]. The hyperfine hamiltonian matrix elements of the $J = 1, K_{-1} = 1$ state can be written as [46]:

$$\begin{aligned}
 E/h = & C(-1)^{I+J+F}[I(I+1)(2I+1)J(J+1)(2J+1)]^{1/2} \\
 & \times \left\{ \begin{array}{ccc} F & I & J \\ 1 & J & I \end{array} \right\} + D(-1)^{I+J+F} \left\{ \begin{array}{ccc} F & I & J \\ 2 & J & I \end{array} \right\} \\
 & \times \left[\frac{(I+1)(2I+1)(2I+3)J(J+1)(2J+1)}{I(2I-1)(2J-1)(2J+3)} \right]^{1/2},
 \end{aligned} \tag{1}$$

where $I = 1$ is the sum of proton spins, J the rotational angular momentum, $F = J + I$ the total angular momentum, C the spin-rotation interaction constant and D the spin-spin interaction constant. Substituting $C(1_{11}) = -3.07$ kHz and $D(1_{11}) = 8.87$ kHz [46] for the lower state $K_1 = 1$ we obtain the hamiltonian matrix elements in the $|F, m_F\rangle$ representation. After transforming to the $|m_J, m_I\rangle$ basis as:

$$|m_J, m_I\rangle = \sum_{F, m_F} \langle F, m_F | m_J, m_I \rangle |F, m_F\rangle, \tag{2}$$

the hamiltonian is diagonalized to obtain the time evolved states [32] shown in Fig. 3, where at $t_{max} = 16.2 \mu\text{s}$, 15.9% of the population has been transferred to the $m_J = -1$ state, which is always fully nuclear-spin-polarized (Fig. 3(b)). The $\langle m_I \rangle$ of each m_J state is plotted (Fig. 3(c,d)), giving the degree of nuclear polarization for each state.

The same technique can be applied to singly deuterated formaldehyde, CHDO. The effective hyperfine hamiltonian for asymmetric top molecules

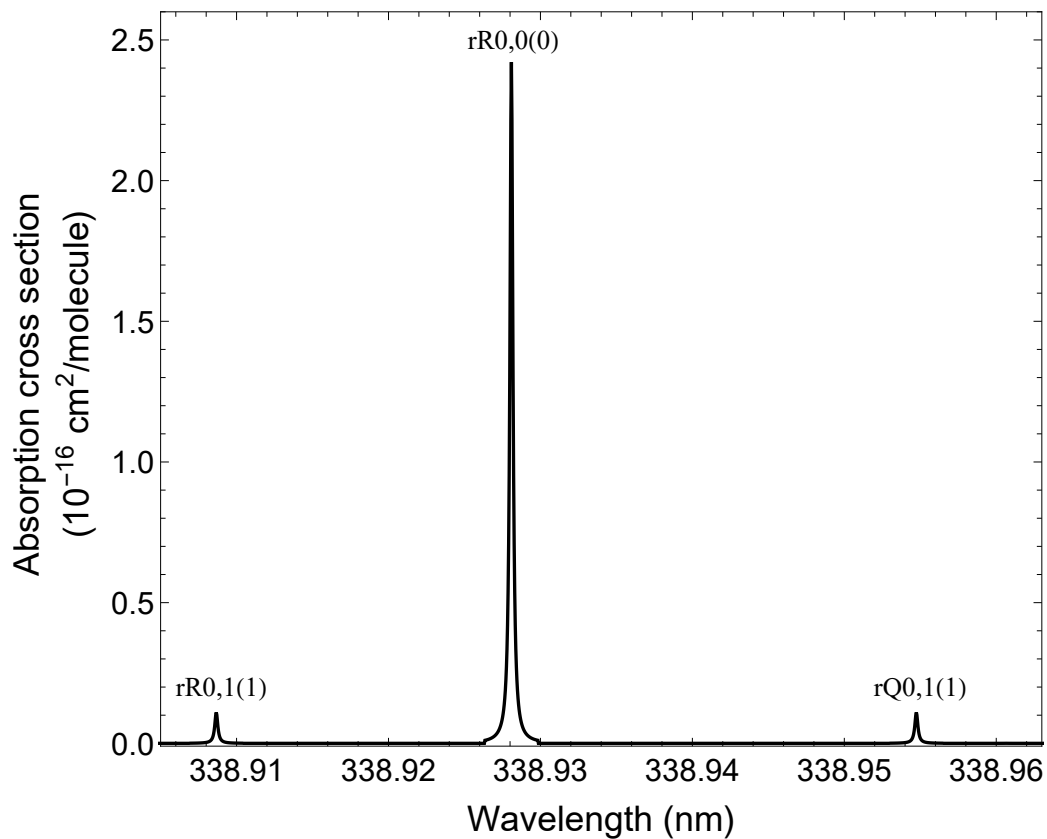


Figure 4: Simulated absorption spectrum of the $2_0^1 4_0^1$ vibronic band of formaldehyde, using Gaussian and Lorentzian FWHM of 0.003 cm^{-1} and 0.02 cm^{-1} , respectively, and $T = 1$ K. Relevant transitions are labeled. The absorption spectrum simulation of the $2_0^1 4_0^1$ vibronic band was performed using the PGOPHER [47] program and the supporting material provided by [48].

with two (nonzero) nuclear spins is written as [49]:

$$\begin{aligned}
H/h = & \frac{(eq_J Q)_D}{2I_D(2I_D - 1)J(2J - 1)} \left[3(\vec{I}_D \cdot \vec{J})^2 + \frac{3}{2}(\vec{I}_D \cdot \vec{J}) \right. \\
& \left. - \vec{I}_D^2 \vec{J}^2 \right] + \frac{d'_J}{J(2J - 1)} \left[\frac{3}{2}(\vec{I}_D \cdot \vec{J})(\vec{I}_H \cdot \vec{J}) \right. \\
& \left. + \frac{3}{2}(\vec{I}_H \cdot \vec{J})(\vec{I}_D \cdot \vec{J}) - (\vec{I}_H \cdot \vec{I}_D)\vec{J}^2 \right] \\
& + C_H \vec{I}_H \cdot \vec{J} + C_D \vec{I}_D \cdot \vec{J},
\end{aligned} \tag{3}$$

where $(eq_J Q)_D$, d'_J , C_H , and C_D are the quadrupole interaction coupling constant, the nuclear spin-spin interaction coupling constant, the proton and deuteron spin-rotation interaction coupling constants, defined in [49].

The hyperfine structure of the 1_{11} and 1_{10} states of CHDO has been studied by Tucker et al. [50]. We investigate the polarization dynamics of the 1_{10} . Substituting $C_H = -1.43$ kHz, $C_D = 0.11$ kHz given in [50], $d'_J = -0.54$ kHz which is calculated from molecular geometry (as it is presented in Fig. 2 of [51]), and $(eq_J Q)_D = 17$ kHz, where the χ_{aa} , χ_{bb} , and χ_{cc} are taken from Table V of [51]. Following the polarization scheme presented in Fig. 2(a), we achieve 21.4% of population with 100% deuteron polarization at $7.9 \mu\text{s}$ (see Fig. 3(c,d)).

To produce nuclear-spin-polarized HD or DT molecules, a different scheme (Fig. 2) is required. Starting with $m_J=2$ ($t=0$), at time $t=t_{max}$ the population of the $m_J = -1$ state is maximized (which has 100% nuclear-spin-polarization), and is then excited to the $J=1$, $m_J = +1$ state. For the calculation of t_{max} the hyperfine constants for the $J=2$ state are needed. However, the $C_{H,D}$ values found in the literature [49, 51, 50] are not consistent and the $M_{gg}^{H,D}$ have not been measured. Thus, we cannot accurately determine t_{max} unless all the hyperfine constants of CHDO are known. The proton spin-rotation constants are particularly required, because they are mainly responsible for the polarization transfer to the proton. In the case of D, the corresponding quadrupole coupling interaction is dominating.

3. Production of spin-polarized H₂ (isotopes) from formic acid IR excitation and photodissociation

Similar methods can be applied to ortho-trans-formic acid and isotopes. The effective hyperfine hamiltonian of formic acid (CH₂O₂) is written as [49,

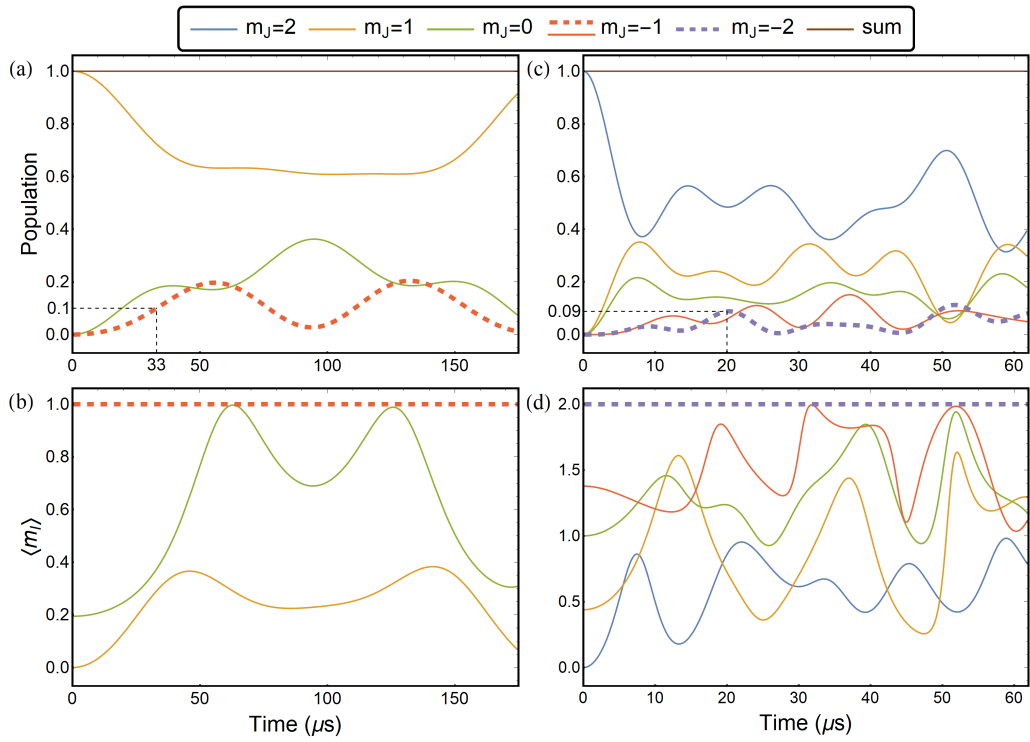


Figure 5: CH₂O₂(a,b): Population and total $\langle m_J \rangle$ of m_J states as function of time. The $m_J = -1$ state reaches 10% of the total population at 33 μs . CD₂O₂(c,d): Population and total $\langle m_J \rangle$ of m_J states as function of time. The $m_J = -2$ state reaches 8.8% of the total population at $\sim 20 \mu\text{s}$.

52, 53]:

$$\begin{aligned}
H/h = & C_{H_1} \vec{I}_1 \cdot \vec{J} + C_{H_2} \vec{I}_2 \cdot \vec{J} \\
& + \frac{d'_J}{J(2J-1)} \left[\frac{3}{2} (\vec{I}_1 \cdot \vec{J})(\vec{I}_2 \cdot \vec{J}) \right. \\
& \left. + \frac{3}{2} (\vec{I}_2 \cdot \vec{J})(\vec{I}_1 \cdot \vec{J}) - (\vec{I}_1 \cdot \vec{I}_2) \vec{J}^2 \right],
\end{aligned} \tag{4}$$

where $I_1 = I_2 = 1/2$, $d'_J = -\frac{6\mu_N^2 g_H^2}{(J+1)(2J+3)r^3} \sum_g \frac{r_g^2}{r^2} \langle J_g^2 \rangle - \frac{1}{3} J(J+1)$, $C_{H_{1,2}} = \sum_g \frac{M_{gg}^{1,2} \langle J_g^2 \rangle}{J(J+1)}$, and the constants labeled with 1 refer to the proton bounded to the carbon atom. For the 1_{11} state, $C_{H_1} = -3.8$ kHz, $C_{H_2} = -4.1$ kHz [53], and $d'_J = 1.8$ kHz [54, 55]. Figure 5 shows that the population of the $m_J = -1$ state reaches 10% at $t \sim 33 \mu\text{s}$, assuming 100% rotational polarization at $t = 0$.

The same technique, but for the $|\nu', J = 2\rangle$ state (Fig. 2(b)) can be applied to double deuterated formic acid (CD_2O_2). The total wavefunction is symmetric in the exchange of nuclear spins I_1 and I_2 . In the case of $K_{-1} = \text{even}$ states, the rotation wavefunction is symmetric, so the nuclear spin wavefunction must be symmetric, i.e. $I = I_1 + I_2 = 0, 2$ (ortho states). Therefore, the non-zero hamiltonian matrix elements in the $|J, I, F\rangle$ representation are [51]:

$$\begin{aligned}
\langle J, I, F | H/h | J, I, F \rangle = & C_D \frac{A}{2J(J+1)} + \left[a_Q \frac{3I(I+1) - 11}{(2I-1)(2I+3)} \right. \\
& \left. + a_S \frac{I(I+1) + 8}{2(2I-1)(2I+3)} \right] \frac{3A(A-1) - 4I(I+1)J(J+1)}{2J(J+1)(2J-1)(2J+3)}, \\
\langle J, I, F | H/h | J, I-2, F \rangle = & \frac{3(2a_Q - a_S)}{8J(J+1)(2J-1)(2J+3)(2I-1)} \\
& \times \sqrt{\frac{(I+3)(3-I)(I+2)(4-I)}{(2I-3)(2I+1)}} [(J-F+I)(J+F+I+1) \\
& \times (F+I-J)(J+F-I+1)(J-F+I-1)(J+F+I) \\
& \times (F+I-1-J)(J+F-I+2)]^{1/2},
\end{aligned} \tag{5}$$

where $A = J(J+1) + I(I+1) - F(F+1)$. The constants a_Q , a_S , and C_D are the quadrupole interaction coupling constant, the nuclear spin-spin interaction coupling constant, and the spin-rotation interaction coupling constant, defined in [51].

Cazzoli et al. [56] measured the hyperfine constants χ_{gg} and calculated M_{gg} (see cc-pCVQZ calculation) using a semi-experimental equilibrium geometry. Figure 5(c,d) shows the hyperfine beats of the 2_{21} state which is initially rotationally polarized. The values of the hyperfine constants are $a_Q = -152.85$ kHz, $a_S = 0.24$ kHz, and $C_D = -2.85$ kHz. The 8.8% of the population has been transferred to the $m_J = -2$ state, at $t_{max} = 20$ μ s. This state is always fully nuclear-spin-polarized (Fig. 5(c,d)).

We have described the production of spin-polarized molecular photofragments from the IR-excitation and photodissociation of molecular beams, with rates that may approach the IR-photon production rates of 10^{21} photons s^{-1} . Details on the production of spin-polarized H_2 and H_2O isotopes, from CH_2O and CH_2O_2 , have been given. The production rates of such method are mainly limited by the efficiency of the IR-excitation, and UV-photodissociation, and trapping steps. We have given arguments that the efficiencies of these steps can be high, however since the scale is so far beyond what has already been demonstrated, proof-of-principle demonstrations of these are necessary to verify to what extent they can be achieved. The point of this paper is to motivate such experimental demonstrations. In addition, future improvements in the power of IR and UV lasers will allow further increases in the production rates of this method.

This method of macroscopic production of polarized molecules can be generalized to several other systems, such as for spin-polarized O_2 , N_2 , NO , and ^{13}CO , from the IR-excitation and photodissociation of O_3 , N_2O , NO_2 , and CO_2 .

This work is supported in part by the Hellenic Foundation for Research and Innovation (HFRI) and the General Secretariat for Research and Technology (GSRT), through the grant agreement No. HFRI-FM17-3709 (project NUPOL).

References

- [1] E. Steffens, W. Haeberli, Polarized gas targets, Rep. Prog. Phys. 66 (11) (2003) 1887–1935. doi:10.1088/0034-4885/66/11/r02.
- [2] M. E. Halse, Perspectives for hyperpolarisation in compact nmr, TrAC, Trends Anal. Chem. 83 (2016) 76–83, sI: Compact NMR. doi:https://doi.org/10.1016/j.trac.2016.05.004.

- [3] M. E. Merritt, C. Harrison, W. Mander, C. R. Malloy, A. Dean Sherry, Dipolar cross-relaxation modulates signal amplitudes in the 1h nmr spectrum of hyperpolarized [13c]formate, *J. Magn. Reson.* 189 (2) (2007) 280–285. doi:<https://doi.org/10.1016/j.jmr.2007.09.011>.
- [4] E. M. M. Weber, D. Kurzbach, D. Abergel, A dnp-hyperpolarized solid-state water nmr maser: observation and qualitative analysis, *Phys. Chem. Chem. Phys.* 21 (2019) 21278–21286. doi:[10.1039/C9CP03334C](https://doi.org/10.1039/C9CP03334C).
- [5] E. ter Haar, W. G. Clark, Brute force nuclear polarization of D₂, *J. Low Temp. Phys.* 94 (1994) 361–371. doi:[10.1007/BF00754675](https://doi.org/10.1007/BF00754675).
URL <https://doi.org/10.1007/BF00754675>
- [6] G. Hupin, S. Quaglioni, P. Navrátil, Ab initio predictions for polarized deuterium-tritium thermonuclear fusion, *Nat. Commun.* 10 (2019) 351.
- [7] M. Temporal, V. Brandon, B. Canaud, J. Didelez, R. Fedosejevs, R. Ramis, Ignition conditions for inertial confinement fusion targets with a nuclear spin-polarized DT fuel, *Nucl. Fusion* 52 (10) (2012) 103011. doi:[10.1088/0029-5515/52/10/103011](https://doi.org/10.1088/0029-5515/52/10/103011).
URL <https://doi.org/10.1088/0029-5515/52/10/103011>
- [8] K. Grigoryev, N. Chernov, R. Engels, I. Ivanov, S. Kiselev, E. Komarov, L. Kotchenda, P. Kravtsov, L. Kroell, A. Martyushov, M. Marusina, M. Mikirtychyants, N. Nikolaev, F. Rathmann, H. P. gen Schieck, S. Sherman, H. Ströher, V. Trofimov, A. Vasilyev, M. Vznuzdaev, Double polarized dd-fusion experiment, *J. Phys. Conf.* 295 (2011) 012168. doi:[10.1088/1742-6596/295/1/012168](https://doi.org/10.1088/1742-6596/295/1/012168).
URL <https://doi.org/10.1088/1742-6596/295/1/012168>
- [9] R. M. Kulsrud, *Application of Polarized Nuclei to Fusion*, Springer US, Boston, MA, 1987, pp. 169–178. doi:[10.1007/978-1-4757-5930-3_14](https://doi.org/10.1007/978-1-4757-5930-3_14).
URL https://doi.org/10.1007/978-1-4757-5930-3_14
- [10] R. W. Moir, Hylife-II inertial fusion energy power plant design, *Fusion Technol.* 21 (3P2A) (1992) 1475–1486. doi:[10.13182/FST92-A29929](https://doi.org/10.13182/FST92-A29929).
URL <https://doi.org/10.13182/FST92-A29929>
- [11] J. H. Ardenkjaer-Larsen, B. Fridlund, A. Gram, G. Hansson, L. Hansson, M. H. Lerche, R. Servin, M. Thaning, K. Golman, Increase

- in signal-to-noise ratio of $> 10,000$ times in liquid-state NMR., *Proc. Natl. Acad. Sci. USA* 100 (18) (2003) 10158–10163. doi:10.1073/pnas.1733835100.
URL <https://doi.org/10.1073/pnas.1733835100>
- [12] A. C. Pinon, A. Capozzi, J. H. Ardenkjær-Larsen, Hyperpolarized water through dissolution dynamic nuclear polarization with UV-generated radicals., *Commun. Chem.* 3 (2020) 57. doi:10.1038/s42004-020-0301-6.
URL <https://doi.org/10.1038/s42004-020-0301-6>
- [13] Y. Shestakov, D. Nikolenko, I. Rachek, D. Toporkov, A. Yurchenko, Nuclear-polarized hydrogen/deuterium molecular source, *Phys. Part. Nuclei* 50 (5) (2019) 513–519. doi:10.1134/S1063779619050204.
- [14] T. Kravchuk, M. Reznikov, P. Tichonov, N. Avidor, Y. Meir, A. Bekkerman, G. Alexandrowicz, A magnetically focused molecular beam of ortho-water, *Science* 331 (6015) (2011) 319–321. doi:10.1126/science.1200433.
URL <https://science.sciencemag.org/content/331/6015/319>
- [15] J. Vermette, I. Braud, P.-A. Turgeon, G. Alexandrowicz, P. Ayotte, Quantum state-resolved characterization of a magnetically focused beam of ortho-h₂o, *J. Phys. Chem. A* 123 (42) (2019) 9234–9239, PMID: 31577429. doi:10.1021/acs.jpca.9b04294.
- [16] T. P. Rakitzis, Highly spin-polarized atoms and molecules from rotationally state-selected molecules, *Phys. Rev. Lett.* 94 (2005) 083005. doi:10.1103/PhysRevLett.94.083005.
URL <https://link.aps.org/doi/10.1103/PhysRevLett.94.083005>
- [17] L. Rubio-Lago, D. Sofikitis, A. Koubenakis, T. P. Rakitzis, Time-dependent polarization transfer from molecular rotation to nuclear spin, *Phys. Rev. A* 74 (2006) 042503. doi:10.1103/PhysRevA.74.042503.
URL <https://link.aps.org/doi/10.1103/PhysRevA.74.042503>
- [18] D. Sofikitis, L. Rubio-Lago, M. R. Martin, Davida J. Ankeny Brown, Nathaniel C.-M. Bartlett, R. N. Zare, T. P. Rakitzis, Preparation of highly polarized nuclei: Observation and control of time-dependent

- polarization transfer from H^{35}Cl molecular rotation to ^{35}Cl nuclear spin, *Phys. Rev. A* 76 (2007) 012503. doi:10.1103/PhysRevA.76.012503.
URL <https://link.aps.org/doi/10.1103/PhysRevA.76.012503>
- [19] D. Sofikitis, L. Rubio-Lago, M. R. Martin, D. J. Ankeny Brown, N. C.-M. Bartlett, A. J. Alexander, R. N. Zare, T. P. Rakitzis, Optical control of ground-state atomic orbital alignment: Cl ($^2\text{P}_{3/2}$) atoms from HCl ($v=2, J=1$) photodissociation, *J. Chem. Phys.* 127 (14) (2007) 144307. doi:10.1063/1.2772272.
URL <https://doi.org/10.1063/1.2772272>
- [20] R. Engels, M. Gaißer, R. Gorski, K. Grigoryev, M. Mikirtychyants, A. Nass, F. Rathmann, H. Seyfarth, H. Ströher, P. Weiss, L. Kochenda, P. Kravtsov, V. Trofimov, N. Tschernov, A. Vasilyev, M. Vznuzdaev, H. P. g. Schieck, Production of hyperpolarized H_2 molecules from \vec{h} atoms in gas-storage cells, *Phys. Rev. Lett.* 115 (2015) 113007. doi:10.1103/PhysRevLett.115.113007.
URL <https://link.aps.org/doi/10.1103/PhysRevLett.115.113007>
- [21] S. B. Mirov, I. S. Moskalev, S. Vasilyev, V. Smolski, V. V. Fedorov, D. Martyshkin, J. Peppers, M. Mirov, A. Dergachev, V. Gapontsev, Frontiers of mid-IR lasers based on transition metal doped chalcogenides, *IEEE J. Sel. Top. Quantum Electron.* 24 (5) (2018) 1–29. doi:10.1109/JSTQE.2018.2808284.
- [22] A. G. Suits, S. D. Chambreau, S. A. Lahankar, State-correlated DC slice imaging of formaldehyde photodissociation: roaming atoms and multichannel branching, *Int. Rev. Phys. Chem.* 26 (4) (2007) 585–607. doi:10.1080/01442350701589908.
URL <https://doi.org/10.1080/01442350701589908>
- [23] Y. Ma, J. Liu, F. Li, F. Wang, T. N. Kitsopoulos, Roaming dynamics in the photodissociation of formic acid at 230 nm, *J. Phys. Chem. A* 123 (17) (2019) 3672–3677. doi:10.1021/acs.jpca.9b00724.
URL <https://doi.org/10.1021/acs.jpca.9b00724>
- [24] D. J. Nesbitt, High-resolution, direct infrared laser absorption spectroscopy in slit supersonic jets: Intermolecular forces and

- unimolecular vibrational dynamics in clusters, *Annu. Rev. Phys. Chem.* 45 (1) (1994) 367–399. doi:10.1146/annurev.pc.45.100194.002055.
- [25] K. Bergmann, H.-C. Nägerl, C. Panda, G. Gabrielse, E. Miloglyadov, M. Quack, G. Seyfang, G. Wichmann, S. Ospelkaus, A. Kuhn, S. Longhi, A. Szameit, P. Pirro, B. Hillebrands, X.-F. Zhu, J. Zhu, M. Drewsen, W. K. Hensinger, S. Weidt, T. Halfmann, H.-L. Wang, G. S. Paraoanu, N. V. Vitanov, J. Mompart, T. Busch, T. J. Barnum, D. D. Grimes, R. W. Field, M. G. Raizen, E. Narevicius, M. Auzinsh, D. Budker, A. Pálffy, C. H. Keitel, Roadmap on STIRAP applications, *J. Phys. B: At. Mol. Opt. Phys.* 52 (20) (2019) 202001. doi:10.1088/1361-6455/ab3995.
URL <https://doi.org/10.1088/1361-6455/ab3995>
- [26] N. V. Vitanov, A. A. Rangelov, B. W. Shore, K. Bergmann, Stimulated raman adiabatic passage in physics, chemistry, and beyond, *Rev. Mod. Phys.* 89 (2017) 015006. doi:10.1103/RevModPhys.89.015006.
URL <https://link.aps.org/doi/10.1103/RevModPhys.89.015006>
- [27] K. Bergmann, N. V. Vitanov, B. W. Shore, Perspective: Stimulated raman adiabatic passage: The status after 25 years, *J. Chem. Phys.* 142 (17) (2015) 170901. doi:10.1063/1.4916903.
URL <https://doi.org/10.1063/1.4916903>
- [28] N. C.-M. Bartlett, D. J. Miller, R. N. Zare, A. J. Alexander, D. Sofikitis, T. P. Rakitzis, Time-dependent depolarization of aligned HD molecules, *Phys. Chem. Chem. Phys.* 11 (2009) 142–147. doi:10.1039/B814133A.
URL <http://dx.doi.org/10.1039/B814133A>
- [29] N. C.-M. Bartlett, J. Jankunas, R. N. Zare, J. A. Harrison, Time-dependent depolarization of aligned D₂ caused by hyperfine coupling, *Phys. Chem. Chem. Phys.* 12 (2010) 15689–15694. doi:10.1039/C0CP00518E.
URL <http://dx.doi.org/10.1039/C0CP00518E>
- [30] L. F. Phillips, Theoretical cross-sections for resonant exchange of rotational energy in a stark field, *Chem. Phys. Lett.* 291 (1) (1998) 94–100. doi:[https://doi.org/10.1016/S0009-2614\(98\)00524-7](https://doi.org/10.1016/S0009-2614(98)00524-7).
URL <https://www.sciencedirect.com/science/article/pii/S0009261498005247>

- [31] N. R. Hutzler, H.-I. Lu, J. M. Doyle, The buffer gas beam: An intense, cold, and slow source for atoms and molecules, *Chem. Rev.* 112 (9) (2012) 4803–4827, pMID: 22571401. doi:10.1021/cr200362u.
- [32] C. S. Kannis, G. E. Katsoprinakis, D. Sofikitis, T. P. Rakitzis, Nuclear-spin-polarization dynamics of H₂, D₂, and HD molecules in magnetic fields, *Phys. Rev. A* 98 (2018) 043426. doi:10.1103/PhysRevA.98.043426.
URL <https://link.aps.org/doi/10.1103/PhysRevA.98.043426>
- [33] D. Singleton, G. Paraskevopoulos, R. Irwin, UV absorption cross-sections of the monomer and dimer of formic acid, *J. Photochem.* 37 (2) (1987) 209 – 216. doi:[https://doi.org/10.1016/0047-2670\(87\)85001-3](https://doi.org/10.1016/0047-2670(87)85001-3).
URL <http://www.sciencedirect.com/science/article/pii/0047267087850013>
- [34] S. Maeda, T. Taketsugu, K. Ohno, K. Morokuma, From roaming atoms to hopping surfaces: Mapping out global reaction routes in photochemistry, *J. Am. Chem. Soc.* 137 (10) (2015) 3433–3445. doi:10.1021/ja512394y.
URL <https://doi.org/10.1021/ja512394y>
- [35] T. J. Butenhoff, K. L. Carleton, C. B. Moore, Photodissociation dynamics of formaldehyde: H₂ rotational distributions and product quantum state correlations, *J. Chem. Phys.* 92 (1) (1990) 377–393. doi:10.1063/1.458440.
URL <https://doi.org/10.1063/1.458440>
- [36] R. Engels, H. Awwad, K. Grigoryev, L. Huxold, M. Martic, A. Rolofs, W. Sartison, H. Ströher, M. Büscher, A. Vasilyev, L. Kochenda, P. Kravtsov, V. Trofimov, M. Vznudaev, Production and storage of polarized H₂, D₂, and HD molecules, *PoS PSTP2017* (2018) 033. doi:10.22323/1.324.0033.
- [37] K. L. Carleton, T. J. Butenhoff, C. B. Moore, Photodissociation dynamics of formaldehyde: H₂ (v,j) vector correlations, *J. Chem. Phys.* 93 (6) (1990) 3907–3918. doi:10.1063/1.458777.

- [38] T. R. Govers, L. Mattera, G. Scoles, Molecular beam experiments on the sticking and accommodation of molecular hydrogen on a low-temperature substrate, *J. Chem. Phys.* 72 (10) (1980) 5446–5455. doi:10.1063/1.439013.
URL <https://doi.org/10.1063/1.439013>
- [39] A. Honig, Spin-polarized protons and deuterons in hydrogen-isotope solids, *AIP Conf. Proc.* 123 (1) (1984) 1084–1089. doi:10.1063/1.34850.
- [40] A. Nass, C. Baumgarten, B. Braun, G. Ciullo, G. Court, P. Dalpiaz, A. Golendukhin, G. Graw, W. Haeberli, M. Henoch, R. Hertenberg, N. Koch, H. Kolster, P. Lenisa, H. Marukyan, M. Raithel, D. Reggiani, K. Rith, M. Simani, E. Steffens, J. Stewart, P. Tait, T. Wise, The HERMES polarized atomic beam source, *Nucl. Instrum. Meth. A* 505 (3) (2003) 633 – 644. doi:[https://doi.org/10.1016/S0168-9002\(03\)00986-0](https://doi.org/10.1016/S0168-9002(03)00986-0).
- [41] D. Sofikitis, P. Glodic, G. Koumariannou, H. Jiang, L. Bougas, P. C. Samartzis, A. Andreev, T. P. Rakitzis, Highly nuclear-spin-polarized deuterium atoms from the UV photodissociation of deuterium iodide, *Phys. Rev. Lett.* 118 (2017) 233401. doi:10.1103/PhysRevLett.118.233401.
URL <https://link.aps.org/doi/10.1103/PhysRevLett.118.233401>
- [42] D. Sofikitis, C. S. Kannis, G. K. Boulogiannis, T. P. Rakitzis, Ultrahigh-density spin-polarized H and D observed via magnetization quantum beats, *Phys. Rev. Lett.* 121 (2018) 083001. doi:10.1103/PhysRevLett.121.083001.
URL <https://link.aps.org/doi/10.1103/PhysRevLett.121.083001>
- [43] A. K. Spiliotis, M. Xygkis, M. E. Koutrakis, K. Tazes, G. K. Boulogiannis, C. S. Kannis, G. E. Katsoprinakis, D. Sofikitis, T. P. Rakitzis, Ultrahigh-density spin-polarized hydrogen isotopes from the photodissociation of hydrogen halides: new applications for laser-ion acceleration, magnetometry, and polarized nuclear fusion, *Light Sci. Appl.* 10 (2021) 35. doi:10.1038/s41377-021-00476-y.
URL <https://doi.org/10.1038/s41377-021-00476-y>

- [44] A. K. Spiliotis, M. Xygkis, M. Koutrakis, D. Sofikitis, T. P. Rakitzis, Depolarization of spin-polarized hydrogen via spin-exchange collisions with chlorine atoms at ultrahigh density [arXiv:2101.02675](https://arxiv.org/abs/2101.02675).
- [45] P. C. Cross, R. M. Hainer, G. W. King, The asymmetric rotor II. calculation of dipole intensities and line classification, *J. Chem. Phys.* 12 (6) (1944) 210–243. doi:10.1063/1.1723935.
URL <https://doi.org/10.1063/1.1723935>
- [46] S. Kukolich, D. Ruben, Measurement of H₂CO hyperfine structure with a two-cavity maser, *J. Mol. Spectrosc.* 38 (1) (1971) 130 – 135. doi:[https://doi.org/10.1016/0022-2852\(71\)90098-1](https://doi.org/10.1016/0022-2852(71)90098-1).
URL <http://www.sciencedirect.com/science/article/pii/0022285271900981>
- [47] C. M. Western, PGOPHER, a program for rotational, vibrational and electronic spectra, University of Bristol, 2005, <http://pgopher.chm.bris.ac.uk>.
- [48] C. A. Smith, F. D. Pope, B. Cronin, C. B. Parkes, A. J. Orr-Ewing, Absorption cross sections of formaldehyde at wavelengths from 300 to 340 nm at 294 and 245 K, *J. Phys. Chem. A* 110 (41) (2006) 11645–11653. doi:10.1021/jp063713y.
URL <https://doi.org/10.1021/jp063713y>
- [49] P. Thaddeus, L. C. Krisher, J. H. N. Loubser, Hyperfine structure in the microwave spectrum of HDO, HDS, CH₂O, and CHDO: Beams-maser spectroscopy on asymmetric-top molecules, *J. Chem. Phys.* 40 (2) (1964) 257–273. doi:10.1063/1.1725107.
URL <https://doi.org/10.1063/1.1725107>
- [50] K. Tucker, G. Tomasevich, Deuteron quadrupole coupling in formaldehyde, *J. Mol. Spectrosc.* 48 (3) (1973) 475 – 478. doi:[https://doi.org/10.1016/0022-2852\(73\)90111-2](https://doi.org/10.1016/0022-2852(73)90111-2).
URL <http://www.sciencedirect.com/science/article/pii/0022285273901112>
- [51] W. H. Flygare, Experimental determination of the field gradient at the deuteron in formaldehyde, *J. Chem. Phys.* 41 (1) (1964) 206–214. doi:

10.1063/1.1725624.

URL <https://doi.org/10.1063/1.1725624>

- [52] J. Chardon, C. Genty, D. Guichon, J. Theobald, rf spectrum and hyperfine structure of formic acid, *J. Chem. Phys.* 64 (4) (1976) 1437–1441. doi:10.1063/1.432412.
URL <https://doi.org/10.1063/1.432412>
- [53] Cazzoli, G., Puzzarini, C., Stopkowicz, S., Gauss, J., Hyperfine structure in the rotational spectra of trans-formic acid: Lamb-dip measurements and quantum-chemical calculations*, *A&A* 520 (2010) A64. doi:10.1051/0004-6361/201014787.
URL <https://doi.org/10.1051/0004-6361/201014787>
- [54] J. Bellet, A. Deldalle, C. Samson, G. Stenbeckeliers, R. Wertheimer, Étude du spectre de rotation de la molécule d'acide formique: B. Étude de quelques substituons isotopiques. application à la détermination de la structure de la molécule, *J. Mol. Struct.* 9 (1) (1971) 65 – 75. doi:[https://doi.org/10.1016/0022-2860\(71\)85007-X](https://doi.org/10.1016/0022-2860(71)85007-X).
URL <http://www.sciencedirect.com/science/article/pii/002228607185007X>
- [55] W. H. Hocking, The other rotamer of formic acid, cis-HCOOH1, *Z. Naturforsch. A* 31 (9) (1976) 1113 – 1121. doi:<https://doi.org/10.1515/zna-1976-0919>.
URL <https://www.degruyter.com/view/journals/zna/31/9/article-p1113.xml>
- [56] G. Cazzoli, C. Puzzarini, S. Stopkowicz, J. Gauss, The rotational spectrum of trans-DCOOD: Lamb-dip measurements, THz spectroscopy and quantum-chemical calculations, *Chem. Phys. Lett.* 502 (1) (2011) 42 – 47. doi:<https://doi.org/10.1016/j.cplett.2010.12.023>.
URL <http://www.sciencedirect.com/science/article/pii/S0009261410016076>